Ultrafast charge separation and recombination dynamics in lead sulfide quantum dot-methylene blue complexes probed by electron and hole intraband transitions

Ye Yang, William Rodríguez-Córdoba, Tianquan Lian

Department of Chemistry, Emory University, 1515 Dickey Dr. NE, Atlanta, Georgia 30322, USA.

S1. Sample Preparations. Lead sulfide quantum dots (QDs) were prepared following a previously reported procedure.[1] Briefly, 0.45 g of lead (II) oxide (Sigma Aldrich), 2.5 ml of oleic acid and 12.5 ml of 1-octadecene (ODE) were injected in a three-neck flask and heated to 120 °C under a continuous argon flow for two hours. Then, 0.18 ml of hexamethyldisilathiane (Sigma Aldrich) in 5 ml of ODE was injected into this mixture. The resulting solution was kept at 120 °C for 1 minute to allow the formation of the QDs and then quenched by cooling it to room temperature. The solution was poured into a mixture of methanol and hexane (3:1). After the removal of the hexane layer by decantation, the QDs were precipitated by adding acetone to the solution. The PbS QDs were then dissolved in heptanes for the TA studies. To prepare the PbS-MB$^+$ complexes, MB$^+$Cl powder was added into PbS heptane solution. The mixture was sonicated and filtered to remove undissolved MB$^+$. The exact binding mode of MB$^+$ on PbS is not known. The average number of MB$^+$ molecules per PbS QD was estimated from the absorbance of PbS and MB$^+$ in the PbS-MB$^+$ complexes as well as the from the absorbance change in the transient spectra as described in S6.

S2. Ultrafast Visible/NIR Transient Absorption Measurements. The femtosecond TA spectrometer used for this study is based on a regeneratively amplified Ti:sapphire laser system (coherent Legend, 800 nm, 150 fs, 3 mJ/pulse, and 1 kHz repetition rate). Briefly, the 800 nm output pulse from the regenerative amplifier was split in two parts with a 10% beam splitter. The

reflected light, with about 25 μJ/pulse, was attenuated with a neutral density filter (~3 μJ) and focused into a 2 mm thick sapphire window to generate a white light continuum (WLC) probe. After collimation with an off-axis parabolic mirror, the while light was divided into a signal and a reference beam. While the signal beam measures the absorption of the sample, the reference beam is used to normalize the laser intensity fluctuation. The signal was focused into the sample with a second aluminum parabolic mirror. After the sample, the probe beam was collimated and then focused into a fiber-coupled visible or NIR spectrometer. The visible light (400 nm − 800 nm) of the probe was detected using a CMOS sensor (1024 pixels) while the NIR part (800 nm − 1200 nm) was detected with a InGaAs linear diode array (256 pixels). The transmitted fundamental beam, with about 2 mJ/pulse, was split into two equivalent beams. One part was used to pump a tunable IR optical parametric amplifier (OPA) used in the generation of the mid-IR probe light (see below). The second part of the fundamental beam was used as excitation beam and was directed to the main optical delay line. The energy of the pump pulses at the sample was controlled by a variable neutral-density filter wheel to be ~80 nJ/pulse. The pump beam was chopped by a New Focus Model 3501 Chopper at 500 Hz. The Kerr effect signal in neat heptane was also measured to determine the instrument response function and t=0. The temporal chirp has been corrected in all the data shown. The typical instrument response was well represented by a Gaussian function with a full-width-at-half-maximum (FWHM) of 150 fs. The diameter of the pump and probe beams at the sample were 250 and 150 μm, respectively. All experiments were performed at room temperature. During data collection, samples were constantly stirred or translated at a speed of 5 mm/min to avoid photodegradation.

S3. Ultrafast Infrared Transient Absorption Measurements. The tunable femtosecond infrared spectrometer is based on a Clark-MXR IR optical parametric amplifier pumped with 1 mJ/pulse of the 800 nm fundamental beam (obtained from the ultrafast regenerative amplifier), which generate two tunable near-IR pulses from 1.1 to 2.5 μm (signal and idler, respectively). These two beams are combined in a 1-mm-thick $AgGaS_2$ crystal, cut for type II phase matching at 40°, to generate the mid-infrared probe pulses from 3 to 10 μm by difference frequency generation (DFG). The DFG signal was collimated with a 50 cm CaF_2 lens before it was focused into a 200 μm path length cell containing the sample, and at the focal point, it was crossed with the temporally delayed 800 nm excitation pulse. The pump energy was 80 nJ/pulse, and the

diameter of the pump and probe beams at the sample were 300 and 200 μm, respectively. The mid-IR probe was then dispersed in a monochromator and the intensity change of the IR light induced by photoexcitation was monitored as a function of time with a 32-element HgCdTe array detector. The pump beam was chopped by a New Focus Model 3501 Chopper at 500 Hz and its polarization was adjusted at magic angle condition (54.7°) relative to the probe beam. The instrument response function (IRF) of the Vis-pump/Mid-IR-probe spectrometer was determined to have a 230 ± 10 fs full width at half-maximum (FWHM) using a thin silicon wafer, in which absorption of 800 nm photons leads to the instantaneous generation of charge carriers that absorb strongly in the mid-IR region. To avoid spectral and temporal reshaping of the Mid-IR probe by absorption of water vapor and CO_2 in air, the entire pump-probe setup was purged by dried air generated by a FTIR purging gas generator (75–62 Parker-Balston).

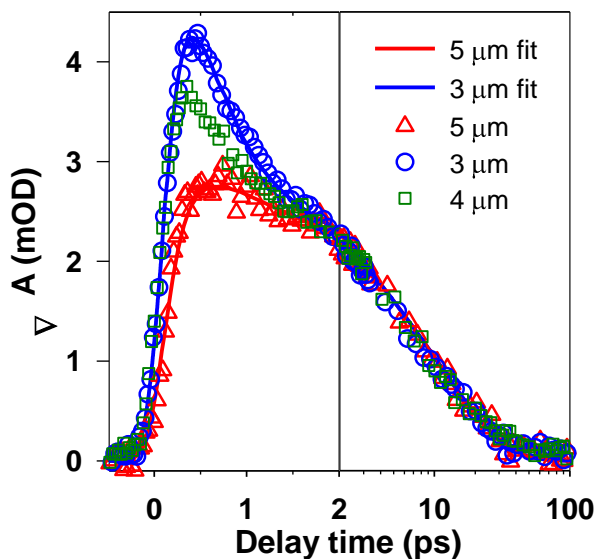## S4. Normalized comparison of mid-IR absorption in PbS-MB$^+$ complexes.

Figure S1. Normalized comparison of kinetics at 3.0 (blue circles), 4.0 (green squares) and 5.0 μm (red triangles) in PbS-MB$^+$. The kinetics at 4.0 and 5.0 μm were normalized to match those at 3.0 μm at later delay times. Solid lines are fits according to equations S4 and S5. The x axis is in linear scale in the left panel (-0.5 – 2 ps) and in logarithmic scale in the right panel (2 – 100 ps).

S5: fitting of kinetics

The kinetics shown in Figure 3 are fit by equation 1. First, the 1S exciton bleach formation and recovery kinetics in free QDs are fit according to equation S1.

$$
\begin{aligned}
\Delta A(930nm, t) &= L(\Delta\varepsilon_e(930nm) + \Delta\varepsilon_h(930nm))[PbS^*](t) \\
&= L(\Delta\varepsilon_e(930nm) + \Delta\varepsilon_h(930nm))N_0(e^{-k_R t} - \sum_i A_i e^{-k_i t})
\end{aligned}
\tag{S1}
$$

where N_0 is the concentration of excited QDs at t=0, L the sample path length, $\Delta\varepsilon_e(930nm)$ and $\Delta\varepsilon_h(930nm)$ are the changes of extinction coefficients at 1S exciton bleach due to the filling of 1S electron and hole levels, respectively. $N_0(\Delta\varepsilon_e + \Delta\varepsilon_h)L$ is the total initial 1S exciton bleach amplitude. A_i, k_i are amplitudes and time constants of the bi-exponential fit to the exciton bleach recovery. The best fit yields a relaxation rate k_R of 5.9×10^{12} s^{-1} in free PbS, which is assumed to be the same for the PbS-MB$^+$ complexes. These fitting parameters are listed in Table S1.

According to equation (1), the concentrations of PbS*-MB$^+$ and PbS$^+$-MB· at time t are given by eq. S2 and S3, respectively:

$$
[PbS^* - MB^+](t) = N_0 \sum_i C_i \frac{k_R}{k_{CSi} - k_R}(e^{-k_R t} - e^{-k_{CSi} t})
\tag{S2}
$$

$$
[PbS^+ - MB\cdot](t) = N_0(\sum_i B_i e^{-k_{CRi} t} + \sum_i C_i(\frac{k_R}{k_{CSi} - k_R}e^{-k_{CSi} t} - \frac{k_{CSi}}{k_{CSi} - k_R}e^{-k_R t}))
\tag{S3}
$$

where B_i, and k_{CRi} are amplitudes and rate constants of the biexponenital function needed to describe the recombination process. C_i and k_{CSi} are the amplitude and rate constant of bi-exponential functions describing the charge separation kinetics.

Because the intraband absorption at 5.0 μm is dominated by the hole $1S_h \rightarrow 1P_h$ transition, its amplitude follows the concentration of 1S holes:

$$\Delta A_{5\mu m}(t) = L\Delta\varepsilon_h(5\mu m) \cdot ([PbS^* - MB^+](t) + [PbS^+ - MB\cdot](t))$$
$$= L\Delta\varepsilon_h(5\mu m) \cdot N_0(\sum_i B_i e^{-k_{CRi}t} - e^{-k_R t}) \tag{S4}$$

The kinetics can be well fit by this model as shown in Figure 3 and 4. The B_i and k_{CRi} values obtained from the fit are listed in Table S2, from which an amplitude weighted average charge recombination rate constant, $k_{ave}=1/\tau_{ave}=(B_1+ B_2)/(B_1 /k_{CR1}+ B_2 /k_{CR2})$, of $1.1\pm0.2\times10^{11}$ is obtained. The error bar is the standard deviation of the charge separation rates determined from three sets of data.

The intraband transition kinetic at 3.0 μm and the 1S exciton bleach at 930 nm contains both the electron and hole contributions:

$$\Delta A(\lambda, t) = L\Delta\varepsilon_e(\lambda) \cdot [PbS^* - MB^+](t) + L\Delta\varepsilon_h(\lambda) \cdot ([PbS^* - MB^+](t) + [PbS^+ - MB\cdot](t))$$
$$= LN_0\Delta\varepsilon_e(\lambda)\sum_i C_i \frac{k_R}{k_{CSi} - k_R}(e^{-k_R t} - e^{-k_{CSi}t}) + LN_0\Delta\varepsilon_h(\lambda)(\sum_i B_i e^{-k_{CRi}t} - e^{-k_R t}) \tag{S5}$$

where $LN_0\Delta\varepsilon_e(\lambda)$ and $LN_0\Delta\varepsilon_h(\lambda)$ are the initial amplitude of the 1S electron and hole induced TA features (1S exciton bleach at 930 nm and intraband transition at 3μm). The second term is the contribution of the 1S hole to the signal, whose kinetics have already been determined by the fit of free QDs 1S hole intraband transition kinetics at 5 μm (eq. S4). We normalized the 1S hole kinetics at 5 μm to the long time signal at these wavelengths. From the normalization factor we determine $LN_0\Delta\varepsilon_h(3\mu m)$ =5.2 mOD and $LN_0\Delta\varepsilon_h(930nm)$ = -12.3 mOD. From the initial amplitudes of the free QD signals at these wavelengths, we can determine the initial amplitude of the electron signals, $LN_0\Delta\varepsilon_e(3\mu m)$ =6.8 mOD and $LN_0\Delta\varepsilon_e(930nm)$ = -5.5 mOD, respectively. The 1S electron kinetics, obtained by subtracting the hole contribution to the kinetics at 3 μm, can of course be fit by the first term in equation S5.

As shown in the transient spectra (Figure 2), the MB^+ ground state bleach overlaps with the charge carrier induced absorption. In order to fit the normalized MB^+ GSB kinetics, the carrier induced absorption should also be considered:

$$\Delta A_{650nm}(t) = L\Delta\varepsilon_1[PbS^* - MB^+](t) + L\Delta\varepsilon_2[PbS^+ - MB\cdot](t)$$

$$= L\Delta\varepsilon_1 N_0 \sum_i C_i \frac{k_R}{k_{CSi} - k_R}(e^{-k_R t} - e^{-k_{CSi} t}) \qquad (S6)$$

$$+ L\Delta\varepsilon_2 N_0 (\sum_i B_i e^{-k_{CRi} t} + \sum_i C_i(\frac{k_R}{k_{CSi} - k_R} e^{-k_{CSi} t} - \frac{k_{CSi}}{k_{CSi} - k_R} e^{-k_R t}))$$

$L\Delta\varepsilon_2 N_0$ is the sum of hole induced absorption and MB^+ bleach at 650 nm. As shown in Figure 3, at > 2ps the normalized kinetics (multiplied by 1.3) at 650 nm agrees well with the kinetics at 930 nm. Because the long time signal is determined by the second term (the charge separated state) only, their amplitudes should agree $LN_0\Delta\varepsilon_2 = LN_0\Delta\varepsilon_h(930nm) = -12.3$ mOD. $L\Delta\varepsilon_1 N_0$ is the initial 1S exciton (both electron and hole) induced TA absorbance change at 650 nm, which can be determined from the transient spectra of free QDs. As shown in Figure 2a, the initial exciton induced absorption at 650 nm is 5.3 mOD. Accounting for the normalization factor (1.3), we determine that $L\Delta\varepsilon_1 N_0 = 6.7$ mOD.

The kinetics at 650, 930 and 3000 nm can be fit simultaneously to equation S5 and S6, with k_{CS} as the only fitting parameter. As shown in Figure 3 and 4, these kinetics can be well fit by this model. The fitting parameters are listed in Table S3. From the best fit parameters, we obtained the charge transfer rate of $2.8\pm0.2\times10^{12}$. The error bar is the standard deviation of the charge separation rates determined from three sets of data.

Table S1. Fitting parameters for kinetics of 1S exciton bleach in free PbS

QD	$L(\Delta\varepsilon_h + \Delta\varepsilon_e) N_0$ (mOD)	$k_R(s^{-1})$	A_1	$k_1(s^{-1})$	A_2	$k_2(s^{-1})$
A_{930nm}	17.8	5.9×10^{12}	-0.13	1.7×10^{11}	-0.87	6.3×10^8

Table S2. Fitting parameters for charge separation kinetics in PbS-MB$^+$

QD-MB*	$L\Delta\varepsilon_h N_0$(mOD)	B_1	$k_{CR1}(s^{-1})$	B_2	$k_{CR2}(s^{-1})$	$k_{CR,ave}(s^{-1})$
$A_{5\mu m}$	4.8	0.70	0.8×10^{12}	0.30	0.6×10^{12}	1.1×10^{11}

*k_R is fixed to the value determined in Table S1.

Table S3. Fitting parameters for charge separation kinetics in PbS-MB$^+$

QD-MB*	$L\Delta\varepsilon_h N_0$	$L\Delta\varepsilon_e N_0$	(s^{-1})	C_1	$k_{CS1}(s^{-1})$	C_2	$k_{CS1}(s^{-1})$	$k_{CS,ave}(s^{-1})$

	(mOD)	(mOD)						
$A_{3\mu m}$	5.2	6.8	5.9×10^{12}	0.40	3.6×10^{12}	0.60	2.4×10^{12}	2.7×10^{12}
A_{930nm}	-12.3	-5.5						
A_{650nm}	$L\varepsilon_1 N_0$ (mOD)	$L\varepsilon_2 N_0$ (mOD)						
	6.7	-12.3						

*Hot electron relaxation and charge recombination rates are fixed to the values determined in table S1 and S2, respectively.

S6. Estimate of MB$^+$:QD ratio.

We estimated the MB$^+$:QD ratio by two methods. The first method is based on the extinction coefficient of MB$^+$ ($7.4\times10^4\,M^{-1}cm^{-1}$ at 660 nm)[2] and PbS ($7.6\times10^4\,M^{-1}cm^{-1}$ at the 1S exciton band),[3] from which the average number of adsorbed MB$^+$ per QD is estimated to be ~1. However, there is considerable error in both extinction coefficients. For MB$^+$, the error is caused by possible aggregations of adsorbed MB$^+$ molecules. The extinction coefficient for the size of PbS QDs studied in this work has not been reported. It was calculated by extrapolating the empirical formula determined for larger size PbS QDs.[3] The value calculated by this method likely underestimates the real ratio based on the appearance of the transient spectra. With an 1:1 average ratio, 36% (or e^{-1}) of QDs in the sample are free of MB$^+$, assuming a Poisson distribution of the number of adsorbates on QDs.[4,5] These free QDs should show long lived (>> 100 ps) 1S exciton bleach. As shown in Figure 2 and 3, at >100 ps the 1S exciton bleach amplitude in PbS-MB$^+$ is less than 1% of that in PbS, suggesting an average MB$^+$:QD ratio m of >4.

In the second method, we determine the relative extinction coefficient of MB$^+$/QD by the relative amplitude of the MB$^+$ bleach at 660 nm and 1S exciton bleach at 930 nm. Under our experimental conditions, most excited QDs are in the long-lived single exciton states.. Because of the ultrafast electron transfer rate, every exciton is dissociated and each exciton generates one reduced MB$^+$ molecule. Therefore, the relative bleach amplitude of these species is determined by their relative extinction coefficient. Due to the 8 fold degeneracy of PbS 1S exciton, the bleach amplitude is related to 1/8 of the extinction coefficient. After correcting for the overlap of the electron and hole induced absorptions at 660 nm (obtained from the fit), we determined that

the relative initial absorbance change of MB (at 660nm)/PbS 1S exciton band (at 930nm) is 13.0/17.8. From the ratio of their absorbance in the UV-visible spectrum (0.93/1), the average number of MB^+ per QD was calculated to be ~10. This estimated ratio is consistent with the negligible long lived exciton bleach in the transient absorption data discussed above. This method yields an exctinction coefficient (at 930 nm) of $7.45 \times 10^5 \, M^{-1} cm^{-1}$ for PbS QDs, 10 times larger than the value extrapolated from the empirical formula (which was determined from larger QDs).[3] The reason for the large discrepancy is unclear.

S7. Average number of excitons per QD.

From the excitation pulse energy, beam size, pathlength (1mm) and the extinction coefficient of PbS QDs ($7.45 \times 10^5 \, M^{-1} cm^{-1}$ at 930 nm), we estimated that the average number of excitons in QDs under our experimental conditions was 0.82. This number can also be estimated from the 1S exciton bleach signal (17.8 mOD) and total 1S exciton absorbance (0.37 OD). Accounting for the 8 fold degeneracy of the 1S exciton transition, this estimate yields an average number of excitons of 0.38, which is in reasonable agreement with the value estimated from photon flux.

References:
(1)   Hines, M. A.; Scholes, G. D. *Advanced Materials* **2003**, *15*, 1844.
(2)   Kamat, P. V.; Dimitrijevic, N. M.; Fessenden, R. W. *Journal of Physical Chemistry* **1987**, *91*, 396.
(3)   Cademartiri, L.; Montanari, E.; Calestani, G.; Migliori, A.; Guagliardi, A.; Ozin, G. A. *Journal of the American Chemical Society* **2006**, *128*, 10337.
(4)   Song, N. H.; Zhu, H. M.; An, S. Y.; Zhan, W.; Lian, T. Q. *ACS Nano* **2010**, *5*, 613.
(5)   Boulesbaa, A.; Huang, Z.; Wu, D.; Lian, T. *Journal of Physical Chemistry C* **2010**, *114*, 962.